LiBeB: A predicted phase with structural and electronic peculiarities

Andreas Hermann,[1,*] B. L. Ivanov,[2] N. W. Ashcroft,[3] and Roald Hoffmann[1]
[1]*Department of Chemistry and Chemical Biology, Cornell University, Ithaca, New York 14853, USA*
[2]*Department of Physics, Vanderbilt University, Nashville, Tennessee 37235, USA*
[3]*Laboratory of Atomic and Solid State Physics, Cornell University, Ithaca, New York 14853, USA*
(Received 4 May 2012; published 10 July 2012)

Beginning an in-depth analysis of binaries and ternaries in the Li-Be-B system, we examine the static structures and electronic properties of LiBeB (i.e., 1:1:1) over a range of pressures. This as-yet unknown compound is predicted to possess a stable ground state at 1 atm and some higher pressures. As the pressure rises, LiBeB goes through a diverse series of structures, beginning with metallic structures, which feature chains and layers of atoms, progressing to structures built on "colorings" of the Laves phases, and containing helical arrangements of boron atoms, on to high-pressure phases that are ternary variants of a body-centered cubic (bcc) lattice. The density of states (DOS) at the Fermi level consistently falls in a pseudogap (sometimes a complete gap is predicted); LiBeB is unlikely to be a good metal or superconductor. The distribution of the DOS follows what electronegativity would predict—Li electrons are transferred to B. Some curious features of the LiBeB structures emerge, including near-icosahedral coordination, independent of atom type; in a range of pressures, a resemblance of the total DOS to that of metallic Be; and also a Dirac surface.

DOI: 10.1103/PhysRevB.86.014104 PACS number(s): 61.50.Ks, 71.20.−b, 81.30.−t, 71.15.Mb

I. INTRODUCTION

In principle, the upper-left corner of the *Periodic Table* should provide an auspicious prospecting ground for superconducting materials: Some of the elements themselves are free electron–like metals and thus feature high electronic densities of states at the Fermi level, and their light masses guarantee high phonon frequencies, and with high Debye temperatures.

The quest for possible metallization and high-temperature superconductivity of hydrogen itself under pressure has already been a long and challenging journey for both theoreticians and experimentalists.[1–3] Helium, the most unreactive of the inert gases, metallizes only at very high pressures.[4–8] Elsewhere, we have studied the Li-H system;[9] we and others have investigated BH_3 under pressure,[10,11] and a variety of Li-B-H compounds.[12–17] Li and Be, immiscible at 1 atm and ordinary temperatures, are predicted to form stable alloys of varying stoichiometry under pressure. Both Li and Be were added as dopants in a computational study of β-rhombohedral boron, to explain the electronic properties of the latter.[18] Layered structures of LiB were predicted to be stable and superconducting;[19] their synthesis has been attempted.[20]

The search for new superconductors was in fact part of the impetus for the exploration of the ternary Li-Be-B system, the first chapter of which, on the simple 1:1:1 stoichiometry, is reported here. As we will learn, the allure of superconductivity proved to be just that, and it is not supported by the computations. However, as will become clear, we were much rewarded in our exploration with a fascinating array of structural and electronic features in this system: a predicted stable ground state compound at P = 1 atm, changing structure drastically with increased pressure; unusual geometrical features such as helices and high coordination numbers reminiscent of transition metal intermetallics; a Dirac surface; an entry point to the combinatorics of body-centered cubic (bcc), hexagonal close packed (hcp), and face-centered cubic (fcc) lattices; and an isoelectronic principle for understanding the electronic structure of such ternary phases. In addition, our work has already stimulated synthetic efforts on binaries and ternaries of Li, Be, and B.

Join us in the exploration of LiBeB. The computational details are given in the Appendix to this paper.

II. SEARCHING FOR STRUCTURES OF LiBeB

Driven by nothing more than an urge for simplicity, we began our search for stable ternary phases with the Li:Be:B stoichiometry of 1:1:1. Other stoichiometries, such as Li_2BeB, will be the subject of a subsequent publication. The combinatorial challenge presented by the availability of three elements is huge, and an example of that will be presented below.

There is a multitude of known ABC structures one could consider for LiBeB. To get oriented, we began with two attractive possibilities—the standard structure of the Half-Heusler compounds, and ternary variants of the MgB_2 structure. The former is known as a diverse family of ternary ABC compounds (they usually contain a transition metal), with a wide range of properties and applications.[21,22] The latter is a layered binary alloy and an extraordinary superconductor;[23] in it, one could imagine replacing the magnesium and every second boron by either Li or Be. There are several ways to do this, and the Supplemental Material ([A1]; see also Refs. 24 and 25 therein) gives more details on some of these.[26]

However, neither of these alternatives, in any isomeric form, turned out to be enthalpically competitive at P = 1 atm or any other pressure studied, when compared with the results from structure searches that we will discuss now.

The genetic algorithm structure searches that we employed (these were implemented in the static approximation; see Appendix for details) then led us to a number of low-enthalpy structures for LiBeB, with three structures emerging as stable in various pressure regions: a structure of $P2_1/m$ symmetry, stable at low pressures up to 15 GPa; an *Ama2* structure favored between 15 GPa and 70 GPa; and a $P3m1$ structure stable at

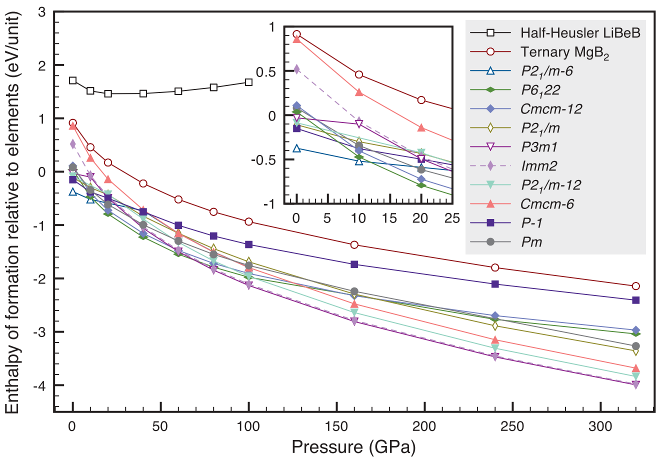

FIG. 1. (Color online) Enthalpies of formation per formula unit for various ground-state and static LiBeB structures, up to pressures of P = 320 GPa. Enthalpies are relative to the enthalpies of elemental crystals. Inset shows low-pressure region.

pressures higher than 70 GPa. Figure 1 shows the enthalpy data of these three and other candidate structures, with the zero of enthalpy taken as that of the respective stable atomic crystal structures. We find that (i) at a pressure of 1 atm, there are several LiBeB structures with negative enthalpies of formation, and (ii) the pressure variable leads to a significant stabilization of other structures.

However, as we discuss next, enthalpic ground state stability with respect to the elements is not necessarily sufficient to guarantee the overall stability of a ternary compound phase.

III. ENTHALPIC STABILITY

The LiBeB phases mentioned here are stable with respect to decomposition into crystals of the respective elements, and increasingly so under pressure, as Fig. 1 shows. That means that the reaction LiBeB(s) $\rightarrow$ Li(s) + Be(s) + B(s) has a positive ΔH (where "(s)" indicates the solid phase). However, other escape routes must be considered, for example, decomposition into binary or other ternary phases. The reaction LiBeB(s) $\rightarrow$ Li(s) + BeB(s) could have a negative ΔH, and so could a more complicated case, such as LiBeB(s) $\rightarrow \frac{1}{4}$ Li(s) + $\frac{1}{4}$ LiBe(s) + $\frac{1}{4}$ Li_2BeB(s) + $\frac{1}{2}$ BeB(s) + $\frac{1}{4}$ B(s). For binary mixtures, an elegant way to present stability of mixtures $A_{1-x}B_x$ is to use "tie-line diagrams," where the convex hull of the enthalpies of formation of $A_{1-x}B_x$, plotted against the atomic ratio x of component B, is constructed. All binary stoichiometries that are part of this convex hull (also called the "global stability line") are stable in their ground states with respect to decomposition into other binary stoichiometries. Similarly, for ternary phase diagrams, the convex hull of the enthalpies of formations of all stoichiometries $A_{1-x-y}B_xC_y$ has to be determined for all atomic ratios x and y of components B and C.[27] Only the compositions defining this convex hull are truly stable compounds (though nothing can be said without further study about kinetic persistence of metastable stoichiometries).[28–30]

For LiBeB, we constructed the ternary convex hull by considering all possible binary mixtures of $Li_{1-x}Be_x$, $Li_{1-x}B_x$, and $Be_{1-x}B_x$, and at all pressures studied. For the LiBe mixtures, which are stabilized under pressure, we took relative stabilities from a recent computational study.[31] For the Li-B and Be-B mixtures, structural data from the ASM Alloy Phase Diagrams Center[32–34] were combined with results from structure searches by us to obtain binary tie-line diagrams at the pressures of interest. Work on other ternary stoichiometries in the Li-Be-B phase diagram is currently in progress (as are experiments on the Li-B and Be-B phase diagrams).

At all pressures, binary compounds of varying stoichiometry are points of stability, as indicated by the vertices along the phase diagram edges in Fig. 2.

But is the ternary LiBeB phase stable with respect to decomposition to *all* possible products? At atmospheric pressure, the ternary $P2_1/m$-6 phase (described later herein) is indeed stable in this sense, as indicated by the existence of the vertex in the center of the ternary phase diagram in Fig. 2, a corner of the hull of enthalpy. At P = 20 GPa, the most stable ternary phase at that pressure is metastable. At P = 80 GPa, however, the low-enthalpy ternary $P3m1$ LiBeB phase is *not* stable. It is part of the phase-separation line connecting pure beryllium and 1:1 stoichiometric LiB. To put it another way, the reaction LiBeB(s) $\rightarrow$ Be(s) + LiB (s) has a negative ΔH at high

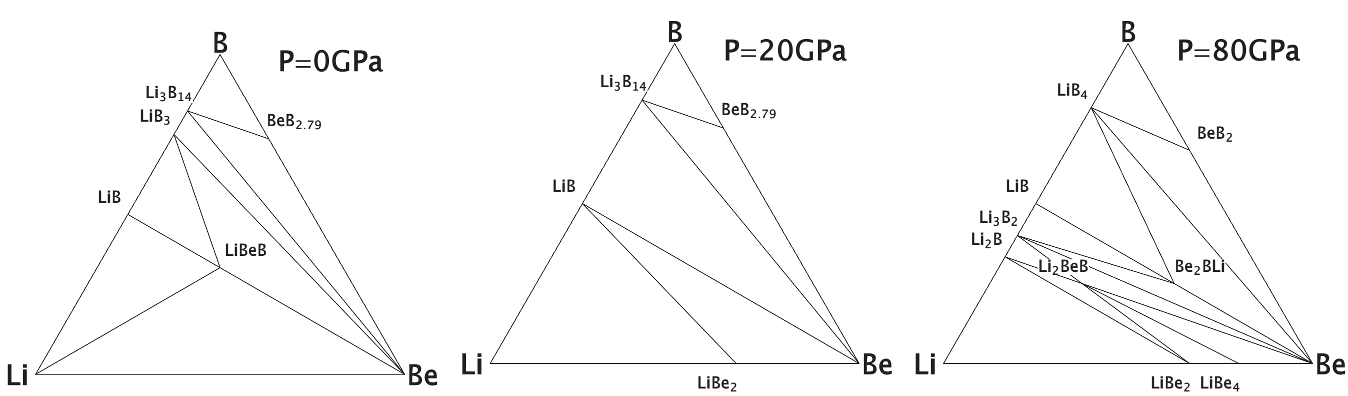

FIG. 2. Ternary phase diagrams for ground-state structures in the Li-Be-B system at various pressures. All labeled vertices indicate calculated stable stoichiometries.

pressures—$\Delta H = -150$ meV per formula unit at $P = 80$ GPa, and $\Delta H = -160$ meV per formula unit at $P = 160$ GPa. As mentioned already, this does not exclude the possibility of preparing metastable, kinetically persistent ternary LiBeB phases; also, the gain in total enthalpy upon decomposition is relatively small. The reason for the relative instability of ternary LiBeB is the formation of very stable binary LiB phases under high pressures, which we will report on elsewhere.

IV. LiBeB AT LOW PRESSURES: LOW-DIMENSIONAL METALLIC STRUCTURES

At low pressures, a $P2_1/m$-*6* phase with six atoms per unit cell is enthalpically favored (at atmospheric pressure by about -0.37 eV per unit of LiBeB). The structure (see Fig. 3, and the Supplemental Material[26] for lattice parameters of this and all other relevant structures) features buckled triangular nets of beryllium and boron, interspersed by lithium; within the BeB sheets, both boron and beryllium form one-dimensional chains. Not only can the crystal structure be dissected into two- and one-dimensional sublattices (see the Supplemental Material[26] for geometrical justification), but the consequences of these features arise in the electronic structure as well, as we will show later herein. Similar sandwich structures of

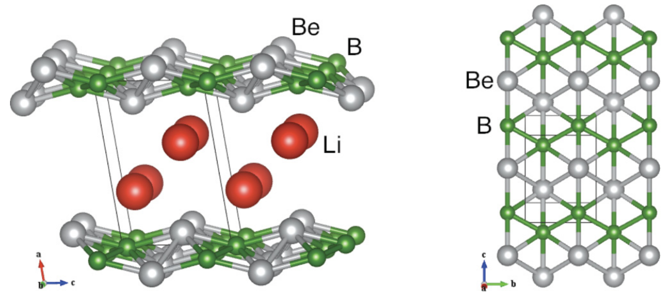

FIG. 3. (Color online) Calculated crystal structure of the $P2_1/m$-*6* phase of LiBeB at P = 1 atm: side-on view (left) and top view (right) of the buckled triangular BeB layers or sheets. Red/silver/green (dark/light/medium gray) spheres denote Li/Be/B atoms, respectively. A monoclinic unit cell of six atoms is indicated. Atoms less than 2.2 Å apart are shown as connected.

BeB sheets alternating with Li layers are found in other low-enthalpy structures at atmospheric pressure, roughly those with a negative enthalpy of formation in Fig. 1. Higher-enthalpy structures feature more close-packed structures, which are in turn stabilized at higher pressures.

In the $P2_1/m$-*6* structure at atmospheric pressure, the shortest separations between like elements are comparable to

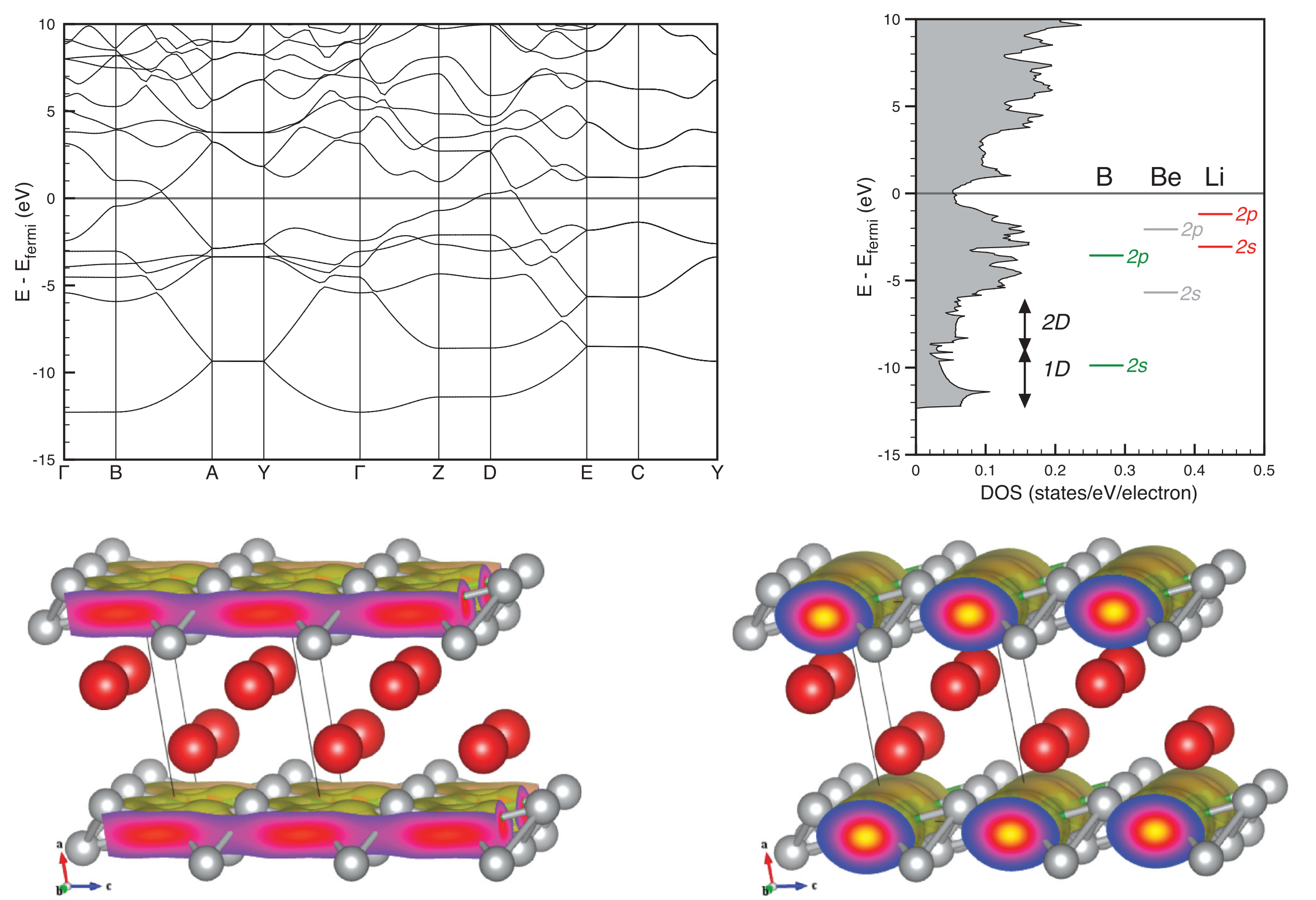

FIG. 4. (Color online) Upper panel: Electronic band structure (left) and DOS per electron (right) of the $P2_1/m$-*6* phase of LiBeB. The DOS plot also indicates atomic energy levels of Li, Be, and B, normalized to the solid's Fermi energy. Lower panel: Charge density isosurfaces ($\rho = 0.01$ e/Å^3) of 2D (left) and 1D features (right), integrated over the respective energy ranges indicated in the DOS plot above.

(but slightly shorter than) their respective bulk materials: B-B separations of 1.74 Å, compared to 1.79 Å in α-boron; Be-Be distances of 2.16 Å, compared to 2.21 Å in hcp-beryllium; and Li-Li separations of 2.92 Å, compared to 3.04 Å in hR9-lithium. Drawing the coordination polyhedra and neighbor distance histograms for all three elements (see Fig. S4 in the Supplemental Material[26]) allows us to recognize the $P2_1/m$-6 phase as a layered structure. This can also be seen by monitoring the energy needed to separate the BeB sheets: Starting from the P = 1 atm geometry, we elongated the a axis while keeping the BeB sheets intact and re-optimizing the Li atoms. The energy needed for complete separation is only 0.3 eV per LiBeB unit.

We are not aware of any other ternary ABC compound with this structure type. The substantially negative enthalpy of formation of LiBeB, and its stability relative to all binary decompositions (see Fig. 2) augurs well for the eventual synthesis of this phase.

The $P2_1/m$-6 phase is metallic. Its band structure and electronic density of states (DOS) per electron are shown in Fig. 4. Between −12 and −8.5 eV below the Fermi energy, the DOS has a typical feature of weakly interacting one-dimensional (1D) chains (a square-root decrease of the DOS after an initial sharp onset), and between −8.5 and −6 eV, it has a typical two-dimensional (2D) structure (plateau of DOS with a square onset). Indeed, if one performs a charge integration restricted to those energy intervals, one obtains the charge densities shown in the lower panel of Fig. 4, clearly indicating the 2D features within the BeB sheets, and the 1D feature along the B chains within these sheets.

The 1D feature at the bottom of the valence band of LiBeB is dominated by boron 2s electrons. This follows from the energies of the 2s and 2p electrons of isolated boron, beryllium, and lithium atoms, shown by the bars at the right in Fig. 4. For both 2s and 2p levels, the energy orders B < Be < Li, an order consistent with a higher effective charge for boron due to ineffective screening by the other electrons in the valence shell. We note that a similar electronic two-dimensionality was found by us before in LiBe and $LiBe_2$, which, however, are only stable under pressures of at least 50 GPa and 15 GPa, respectively.[31]

A feature more relevant to the potential superconductivity of LiBeB is the value of the DOS at the Fermi energy, which is about 0.06 states/eV/electron; this is about twice the value for hcp-beryllium, but only about 12% of the value of bcc-lithium. Or, put another way, in a free electron gas of the same valence bandwidth as LiBeB (about 12.5 eV), the DOS at the Fermi energy would be 0.12 states/eV/electron. Chemistry burns a hole into the DOS around the Fermi energy: not as deep as in pure beryllium, as we see, but enough to render this compound far from a free electron–like metal near the Fermi energy.

V. INTERMEDIATE-PRESSURE PHASES: HELICES

Under pressure, more compact structures than the one we just examined are stabilized in their ground states. Between P = 15 GPa and P = 70 GPa, the structure searches reveal an *Ama2* phase, shown in Fig. 5, as most stable. It can be seen as a hexagonal network of lithium atoms (in an approximation to the hexagonal diamond structure, space group $P6_3/mmc$), with

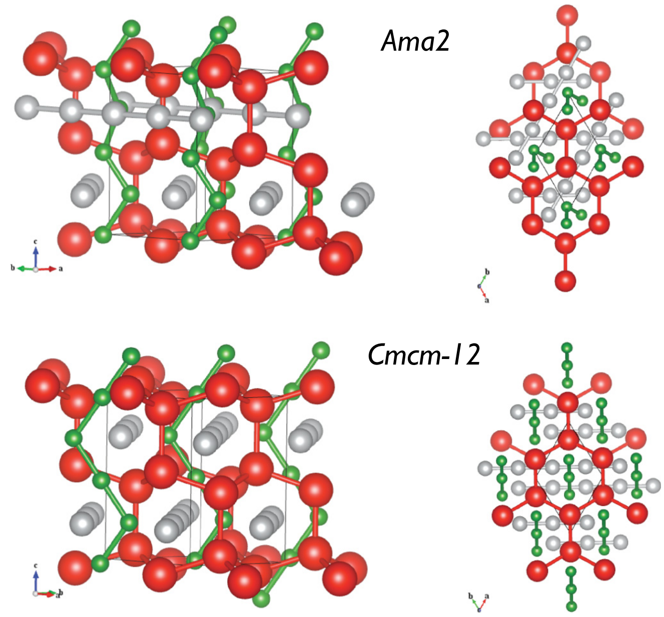

FIG. 5. (Color online) Calculated crystal structure of the intermediate-pressure phases *Ama2* (top) and *Cmcm-12* (bottom) of LiBeB, at P = 40 GPa. Side-on views (left) and top views along the c axes (right) are shown. The connectivity shown follows the structural interpretation given in the text. See caption of Fig. 3 for colors of the atoms.

linear beryllium chains filling its cavities along the $[11\bar{2}0]$ and $[1\bar{2}10]$ directions, and buckled boron chains along the [0001] direction. The latter feature is reminiscent of the structure of the known binary compound LiB, which has hexagonal packing of Li atoms and linear chains of B atoms in cavities along the c axis.[35,36] Only slightly higher in enthalpy than the *Ama2* phase (by about 60 meV per formula unit at P = 40 GPa), a *Cmcm-12* phase has similar features, but all beryllium chains are parallel to each other, as illustrated in Fig. 5.

There is a slightly more efficient way to incorporate the features described here—linear beryllium chains, buckled boron chains, and a hexagonal lithium network—into a crystal structure of LiBeB. By stacking three unit cells of the *Ama2* phase along the c axis and rotating them by 120 degrees with respect to each other, one obtains a $P6_122$ phase with 36 atoms in the unit cell; it is slightly lower in enthalpy than the *Ama2* phase, by about 5 meV per formula unit at P = 40 GPa. Constructed in this way, the $P6_122$ phase has buckled boron chains with a regular precession of the buckling direction around the c axis; the off-axis boron atoms form a 6_1 helix along the c axis (see Fig. 6). The feature of chiral 6_1 chains of face- or edge-sharing polyhedra has been found previously, e.g., in the crystal structures of $CsCuCl_3$[37,38] or AuF_3.[39]

Electronically, these intermediate-pressure structures are metallic; however, the DOS at the Fermi energy is significantly depleted compared to the low-pressure $P2_1/m$-6 phase (see Fig. 6). The electronic structure reflects the low-dimensional structural features—chains of Be and B atoms—discussed earlier herein (see Supplemental Material for more details[26]).

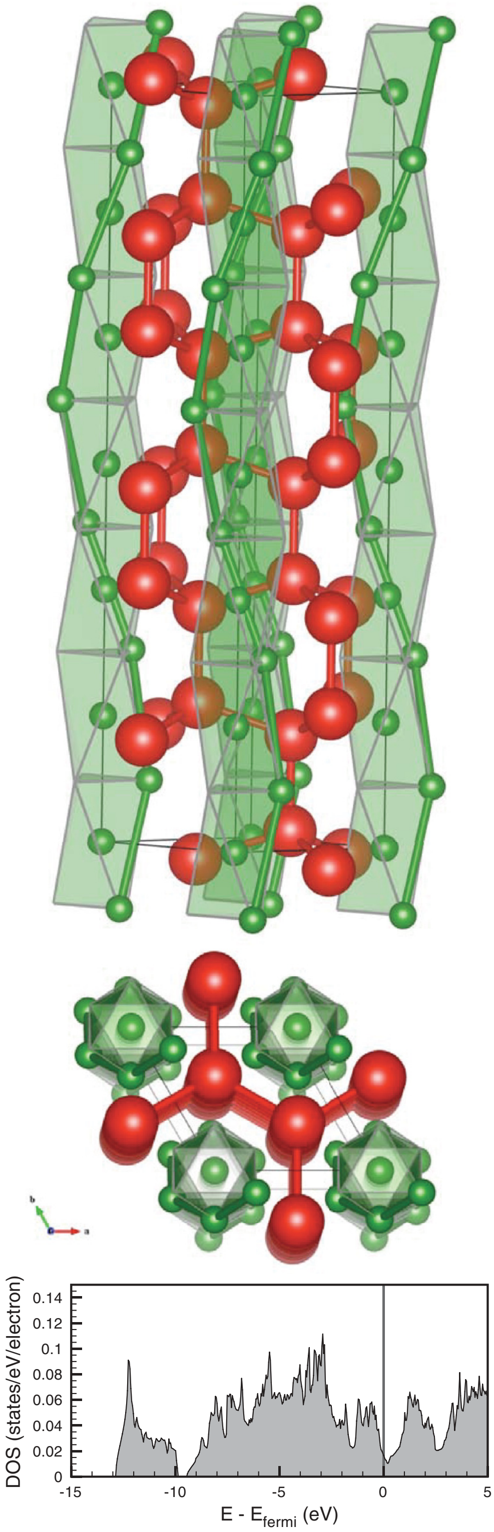

FIG. 6. (Color online) Calculated crystal structure of the $P6_122$ phase of LiBeB. Side view (top) and top view (middle) are shown. Be atoms are omitted, but are on the empty vertices of the boron-centered trigonal antiprisms (shaded green/gray). The boron helix around the c axis is drawn as a guide to the eye. Unit cell is indicated. Bottom shows the electronic DOS per electron at P = 40 GPa, and is low at the Fermi energy.

VI. HIGH COORDINATION AND COLORING A LAVES PHASE

As Fig. 1 shows, the intermediate-pressure regime is dominated by several close-packed phases, which are similar in enthalpy and move in a similar way with pressure. They share the structural features of the hexagonal Laves phases. For these phases, even more than for the previously discussed $P2_1/m$-6 phase, the division into such sublattices can seem arbitrary (even though electronic features we discuss later support this division). In fact, however, they can alternatively be seen as ordered ternary variants of the hexagonal Friauf-Laves phase C14 (prototype $MgZn_2$),[40–42] with lithium occupying the $4f$ Wyckoff position, beryllium partially occupying the $6h$ position, and boron the remaining $6h$ and the $2a$ positions. Accordingly, the coordination polyhedra of the atoms in these phases (see Fig. S5 in the Supplemental Material[26]) are slightly distorted icosahedra for both boron and beryllium (one of these, for one boron site, is shown in Fig. 7) and nominally a Z16 Frank-Kasper polyhedron[43] for lithium.

Given the very unequal size (i.e., as determined by covalent or ionic radii) of the atoms, coordination numbers are to a degree arbitrary (here, we arrive at them by observing natural gaps in neighbor distance histogram plots, which are included in the Supplemental Material[26]). However, these high coordination numbers, and quasi-icosahedral coordinations, lead us to think that we could equally well describe these phases as having high coordination at every atomic site. Note that while lithium is found in other Laves phases, most notably $CaLi_2$,[44–47] this seems to be the first structure where it occupies the "large atom" lattice site of the Laves phase, i.e., the site the X atom occupies in a typical Laves phase XY_2.

Other phases with a hexagonal lithium network intercalated by low-dimensional boron and beryllium structures were found in the structure searches, but with higher enthalpies of formation. There are 70 ways to distribute two different kinds of atoms in 1:1 stoichiometry over the eight $6h$ and $2a$ Wyckoff sites in the primitive unit cell of the C14 structure type—or, in other words, to "color" the $2a$ and $6h$ sites with two colors.[48–50] Nine of these are of unique symmetry.[51] We optimized all of these combinations at P = 40 GPa, and found

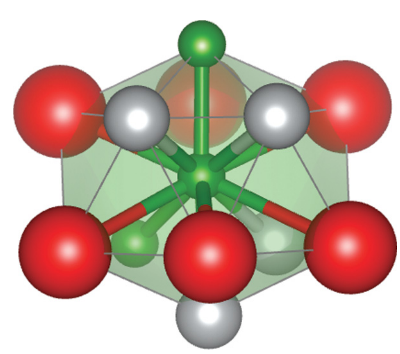

FIG. 7. (Color online) Coordination polyhedron of one of two unique boron sites in the $Ama2$ phase, at P = 40 GPa. All distances from central boron atoms lie between 1.9 Å and 2.3 Å. See caption of Fig. 3 for colors of the atoms.

that the *Ama2* and *Cmcm-12* phases described previously are indeed the two with the lowest enthalpy; structures and relative enthalpies of all of these ternary Laves phase variants are listed in the Supplemental Material.[26]

However, there are 12,870 ways to distribute two kinds of atoms in the *doubled* unit cell of the C14 structure (doubled along the *c* axis, and containing 24 atoms), 351 of which are symmetry-unique. We systematically optimized these as well and found one phase (also of *Ama2* symmetry) with an enthalpy at P = 40 GPa slightly lower than the *Ama2* structure discussed above—like the latter, it features linear beryllium and buckled boron chains, but the buckled boron atoms go off into different directions off the *c* axis, in an attempt to get as close to a helical arrangement as is possible within the unit cell constraint (see the Supplemental Material for details[26]). This ground-state *Ama2* phase is slightly less stable than the $P6_122$ structure constructed previously.

Going even further, there are 2,704,156 ways to distribute two atoms in the *tripled* unit cell of the C14 structure, but we could not check how many of these are related by symmetry, nor could we calculate their energies. One of these structures is the $P6_122$ phase we described earlier, and extrapolating from the structural trends we saw in the single and double C14 unit cell, it is a plausible candidate for the global enthalpy minimum.

Lastly, one might wonder whether the cubic C15 Laves phase (prototype $MgCu_2$, space group *Fd3m*, 24 atoms in the unit cell) would provide competitive structural candidates for LiBeB.[52] In this phase, the "large" atoms occupy the 8*a* Wyckoff sites and form a diamond-like sublattice, whereas the "small" atoms on 16*d* sites form tetrahedra fused at each vertex and staggered along the *c* direction. Of the 12,870 different ways to distribute Be and B amongst the 16*d* sites, 97 are unique; and all of these are at least 100 meV per formula unit higher in ground-state enthalpy (at P = 40 GPa) than the $P6_122$ structure based on the C14 Laves phase.

Let us move on to higher pressures.

VII. HIGH-PRESSURE PHASES OF LiBeB: INTERPENETRATING CUBIC SUBLATTICES

At pressures higher than P = 70 GPa (relative volume compression about 1.4 for the $P6_122$ phase), still more compact structures are stabilized. The most stable phases at high pressures are *P3m1*, *Imm2*, $P2_1/m$-*12*, and *Cmcm-6* (see Fig. 1; note that the high-pressure $P2_1/m$-*12* and *Cmcm-6* phases differ from the phases $P2_1/m$-*6* and *Cmcm-12* described in the previous paragraphs). All of these are ternary variants of a bcc lattice: All atoms occupy (approximately) bcc lattice sites, with different local arrangements of the two simple cubic sublattices. Under pressure, the constituents seem to resolve for themselves the question of the optimal "coloring" of bcc lattice sites, with equal contribution from three different "colors."[48–50] Indeed, seeing the structures as colorings of the bcc lattice helps us to appreciate the complexity of structural choices available to this ternary.

Studying the cubic sublattices of these phases separately yields some insight into what constitutes the enthalpically favorable structures. For the lowest enthalpy *P3m1* and *Imm2* structures, one cubic sublattice contains boron and lithium

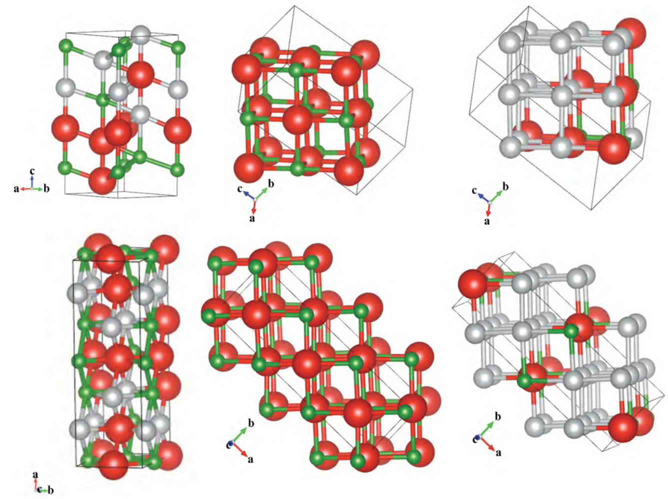

FIG. 8. (Color online) Calculated crystal structure of *P3m1* (top) and *Imm2* (bottom) phases of LiBeB at P = 160 GPa, taken apart into their sublattices. Left: unit cell of complete structure; middle: NaCl-type sublattices of LiB stoichiometry; right: the respective second sublattice of $LiBe_4B$ stoichiometry. The composite structure contains 3 LiB and 1 $LiBe_4B$ sublattices. See caption of Fig. 3 for colors of the atoms.

atoms in a NaCl-type crystal structure, whereas the other sublattice is more complex, featuring all beryllium atoms and the remaining boron and lithium atoms, see Fig. 8. If *all* atoms of the second sublattice were beryllium atoms (this would correspond to the stoichiometry $LiBe_2B$), the structure would be of the well-known Heusler type. Incidentally, in a structure search at that stoichiometry, we found the Heusler phase to indeed be the most stable crystal structure for $LiBe_2B$ at a pressure of P = 80 GPa.

The *P3m1* and *Imm2* phases differ only by little in enthalpy (about 15–30 meV per formula unit over the pressure range 10–320 GPa), because they only differ with respect to the lithium-boron arrangement in the beryllium-dominated sublattice: Li and B form a bilayer in the *P3m1* structure, and isolated linear chains in the *Imm2* phase (see Fig. 8). The conventional cubic unit cell of the *P3m1* phase then contains no less than 432 atoms, or 36 primitive unit cells.

The *Cmcm-6* and $P2_1/m$-*12* phases, somewhat higher in ground-state enthalpy than the two structures just analyzed, exhibit more symmetry. Their conventional cell (the smallest quasi-orthorhombic cell) contains 24 atoms, or 4 primitive unit cells. In Fig. 9, we show their primitive unit cells together with the two simple cubic sublattices of their approximate bcc structures. In both phases, the two sublattices are identical but shifted with respect to each other along the crystalline *c* axis. They contain all three elements in LiBeB stoichiometry.

For the *Cmcm-6* phase, both sublattices contain a two-dimensional square lattice of beryllium atoms that alternates with a simple cubic boron-lithium bilayer. Superimposing the two sublattices, all beryllium atoms are then to be found at the center of a cubic boron-lithium cage. Note that the low-pressure $P2_1/m$-*6* phase transforms into this *Cmcm-6* phase at about P = 40 GPa: Upon compression of the former, the initially well-separated beryllium-boron sheets of the $P2_1/m$-*6*

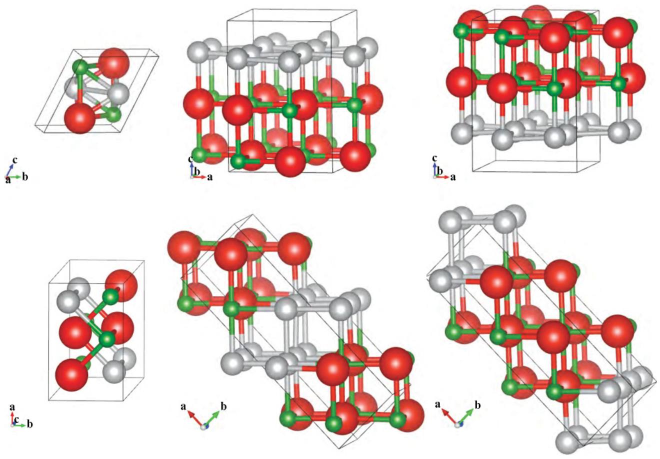

FIG. 9. (Color online) Calculated crystal structures of the *Cmcm-6* (top) and $P2_1/m$-*12* (bottom) phases of LiBeB. Left: primitive unit cell; middle: conventional unit cell with simple cubic sublattice 1; right: conventional unit cell with sublattice 2. See caption of Fig. 3 for colors of the atoms.

phase begin to penetrate the lithium layers and interact, and in the process form the three-dimensional network that is the *Cmcm-6* phase.

For the high-pressure $P2_1/m$-*12* phase, both sublattices also contain all three elements, where layers of beryllium alternate with bilayers of lithium-boron. These layers are orthogonal to the [110] direction of the simple cubic lattice (see Fig. 9; in the *Cmcm-6* phase, they are orthogonal to the [100] direction), and, as in the *Cmcm-6* phase, every beryllium atom in the final structure is found at the center of a lithium-boron cube.

One might argue that ternary "colorings" of other close-packed structures could also yield competitive high-pressure structures for LiBeB. We therefore optimized all the unique crystal structures that are created by placing Li, Be, and B on the lattice sites of an fcc lattice (there are, in fact, 11 unique ways to do this for the 6-atom unit cell we chose) and on the lattice sites of an hcp lattice (there are 1515 unique ways to do this for our 12-atom unit cell). Neither of these structure types provides competitive structures in the high-pressure region ($P \geqslant 100$ GPa): All fcc-based structures were at least 1.2 eV per formula unit higher in ground-state enthalpy, and the hcp-based structures were at least 0.75 eV per formula unit higher than the global minimum, the *P3m1* structure.

Viewing these structures as interpenetrating cubic sublattices should not lead us to think that these are not compact structures. As a histogram of neighbor distances shows (see the Supplemental Material for these[26]), all the atoms in these structures are close to 14 $(8+6)$ coordinate.

VIII. ELECTRONIC STRUCTURE OF THE HIGH-PRESSURE PHASES OF LiBeB

The detailed arrangement of the atoms in these close-packed structures determines their electronic properties. Here we encounter a surprise. While *P3m1* and *Imm2* are semiconductors, the *Cmcm-6* and $P2_1/m$-*12* phases are metallic.

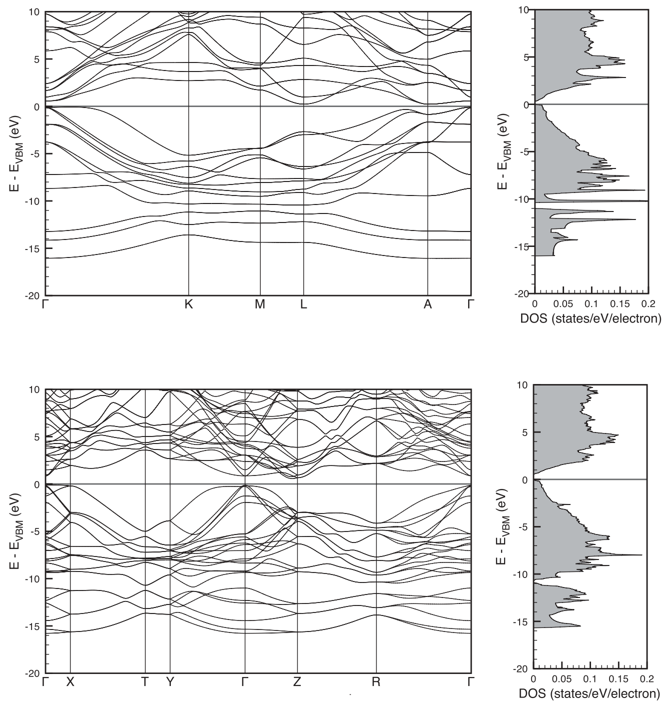

FIG. 10. Band structures and electronic DOS per electron of the *P3m1* (top) and *Imm2* (bottom) phases. All energies are given relative to the valence band maximum (VBM). The orthorhombic unit cell (24 atoms) was used for the *Imm2* phase. A gap above the highest occupied level is quite apparent.

However, neither is as far from the other as that categorization might imply: The band gaps in the *P3m1* and *Imm2* phases at $P = 160$ GPa are only about 0.3 eV and 0.7 eV, respectively, and the Fermi level in the metallic *Cmcm-6* and $P2_1/m$-*12* phases is positioned at a pseudogap and is again severely depleted in states (see Figs. 10 and 11).

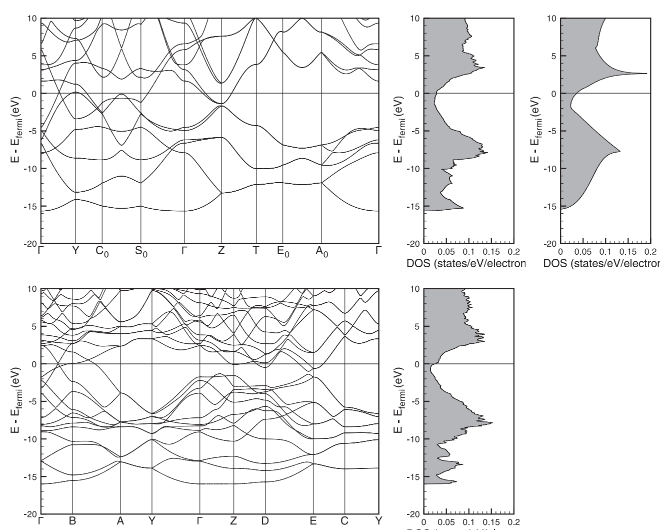

FIG. 11. Band structures and electronic DOS per electron of the *Cmcm-6* (top) and $P2_1/m$-*12* (bottom) phases at $P = 160$ GPa. On the top right, the DOS of bcc-Be at $P = 160$ GPa is shown. All energies are given relative to the Fermi level. Though the band gap has closed, the DOS per electron remains low.

The electronic band gaps in the two semiconducting phases are small over the entire pressure range (see Supplemental Material for the pressure dependence of the band gaps[26]): Their maxima are 0.36 eV at P = 70 GPa for the *P3m1* phase, and 0.7 eV at P = 120 GPa for the *Imm2* phase. The gap in the *P3m1* structure seems to close at the upper end of the pressure range we investigated, at about P = 350 GPa. Note that for this pressure, band gaps obtained from normal DFT calculations can be underestimated.

The detailed features in the band structures and DOSs of the semiconducting phases depend on the microscopic atomic arrangement. For example, the DOS of the *P3m1* phase has several flat bands and corresponding peaks in the DOS—these arise from combinations of localized boron 2*s* orbitals; the lowest three valence bands at E = −16 to −11 eV show only weak dispersion; these are boron-boron bonding orbitals of 2*s* and 2*p* character. These can also be seen in the other close-packed phases, all of which exhibit boron-boron interactions that we classify as bonding based on the interatomic separations and plots of the energy-projected charge densities for these phases (given in the Supplemental Material[26]).

IX. IS LiBeB AT HIGH PRESSURE SIMILAR TO BERYLLIUM?

The DOSs of the two high-pressure metallic phases of LiBeB are very similar to the DOS of pure beryllium (which of course is isoelectronic to LiBeB) in a hypothetical body-centered cubic phase. In the top panel of Fig. 11, we show the DOS of bcc-Be at a pressure of 160 GPa next to the DOS of the *Cmcm-6* phase: The total bandwidth and general features such as the pronounced pseudogap at the Fermi level and maxima at −7 eV and 3 eV are well reproduced. Other details of the electronic structure, such as the peak at −15 eV in the DOS of the *Cmcm-6* phase (which is due to low-lying boron 2*s* states), are, of course, unique to the LiBeB system. Note that pure

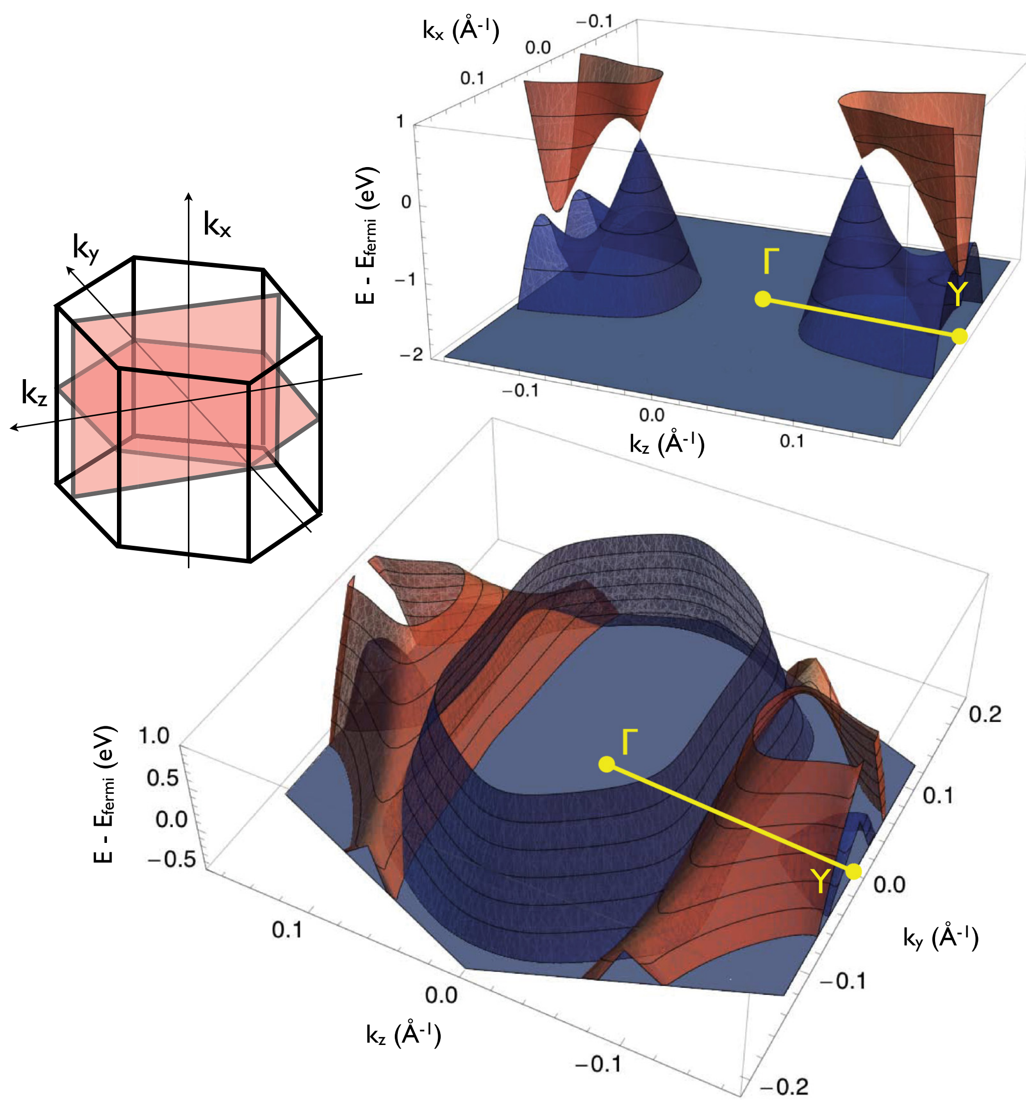

FIG. 12. (Color online) Two-dimensional electronic band structure of the *Cmcm-6* phase at P = 160 GPa in the $k_y = 0.08$ Å^{-1} plane (top) and the $k_x = 0$ plane (bottom). Top left sketches the Brillouin zone and these two planes. Blue (dark gray) and orange (light gray) surfaces depict the electronic bands near the Fermi energy; the underlying gray rectangle and hexagon depict the Brillouin zone. The special path Γ-Y is indicated in both plots.

beryllium has a high-pressure bcc phase that is predicted to be stabilized at around 400 GPa,[53] and has not been found up to 200 GPa.[54] For the isoelectronic LiBeB, the bcc variants discussed here are stabilized at much lower pressures. Since *P3m1* is the most stable of these high-pressure phases, we expect a metal-insulator transition for LiBeB to occur at the stabilization pressure of *P3m1* with respect to *Ama2*, at about P = 70 GPa in the static approximation.

As will be seen in Fig. 13, the Fermi level in LiBeB falls in the deep trough of a pseudogap, something which also happens in the intermediate-pressure phases. This is a not uncommon feature of intermetallic compounds, from the Laves phases to the γ-brasses. If one wants to design a material with a higher DOS, potentially a superconductor, one might want to add or subtract electrons without affecting the underlying crystal structure. For electron doping, and given the electronegativity order of the elements in LiBeB, lithium "doping" comes to mind, for instance, in a hypothetical Li_2BeB. We have studied this hypothetical material in some detail, and other $Li_xBe_yB_z$ stoichiometries as well. With respect to the issue at hand, insertion of additional Li into the LiBeB structure leads to a major change in geometry, and a simple "doping" view will not work, even though we do indeed find enhanced DOS at the Fermi level in Li_2BeB; these and other results will be reported separately.

X. CLOSE TO A DIRAC SURFACE?

The band structure of the *Cmcm-6* phase (top panel of Fig. 11) has an interesting feature: Along the Γ-Y direction, which in our choice of unit vectors is along the path (0,0,0)$\rightarrow$(0,0,1/2) in the Brillouin zone, two electronic bands with linear dispersion cross just above the Fermi energy. Is this close to a "Dirac point"?

Using two different cuts through the Brillouin zone, and plotting within the respective planes the two-dimensional dispersion of the two bands involved, we obtain the following picture (see Fig. 12): Perpendicular to the Γ-Y direction, and within the $k_x = 0$ plane, the two bands cross along a line. In reciprocal coordinates, Y = (0,0,$\pm$0.164) Å^{-1}. Both bands show linear dispersion across a significant part of the Brillouin zone, and especially along their lines of intersection at $k_z = \pm 0.08$ Å^{-1}. While the effective mass is zero along the Γ-Y direction, it is infinite along the k_y direction. Within the $k_y = 0.08$ Å^{-1} plane, we see the conical intersection of the two bands, at $k_x = 0$ and $k_z = \pm 0.08$ Å^{-1} (see Fig. 12). By varying k_y, this cone can be found along the line of intersection of the two bands, throughout most of the Brillouin zone. This conical feature is therefore not a fully three-dimensional "Weyl point,"[55] but is two-dimensional in nature, similar to what is found in graphene,[56] or in ternary Mn-Bi compounds.[57,58]

Note that the conical intersection of the two bands is only about 0.2 eV above the Fermi level. One could imagine that, through doping or uniaxial stress of the *Cmcm-6* unit cell, one might shift the Fermi energy up to coincide with the intersection line of these two bands, and thus the collective of intersection cones.

XI. SUPERCONDUCTIVITY?

Despite a lack of a unifying microscopic theory of superconductivity, several macroscopic observables are found to correlate well with the measured transition temperature T_c: A high density of states at the Fermi level and large electron-phonon coupling are found in a wide variety of superconducting materials, and seem to be crucial properties. In the earliest form of the Bardeen-Cooper-Schrieffer (BCS) theory of phonon-based superconductivity, T_c is proportional to the Debye temperature T_D of the material. Hence, in a qualitative survey, we may simply monitor $N(0)$, the electronic density of states at the Fermi energy E_F, and T_D, the Debye temperature, for the metallic phases of ternary LiBeB.

The density of states at the Fermi level $N(0)$ is shown in Fig. 13 for various low-enthalpy metallic structures. The layered *P2₁/m-6* structure stable at low pressures has a significantly higher $N(0)$ per valence electron than all other, more compact, structures. The latter do not differ much from the (quite depleted) $N(0)$ value of pure beryllium in the hcp phase. Note that in MgB_2 at P = 1 atm, $N(0) = 0.09$ states/eV/electron. For comparison, we have also drawn the DOS of a free electron gas, evaluated at all pressures at the r_s value of the *Ama2* structure: All compounds' DOSs are significantly lower than this ideal case, as hinted at by the prominent pseudogaps in basically all structures. Furthermore, $N(0)$ remains more or less constant over a wide range of pressures. One could not argue from such a flat DOS-vs-pressure relationship for much of a pressure effect on superconductivity.

The Fermi surfaces of the metallic structures are given in Fig. 14: They consist of two or three sheets that generally form elongated protrusions in the Brillouin zone. The "Dirac line" feature in the band structure of the *Cmcm-6* phase results in two parallel Fermi surface lines along the k_y direction, as seen in the blue (dark-gray) sheet in Fig. 14.

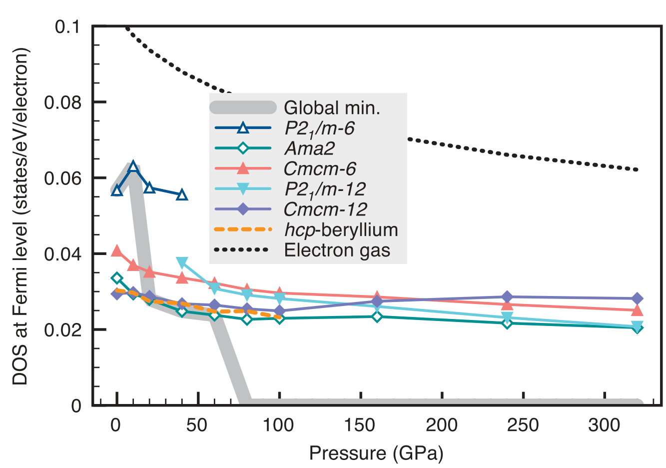

FIG. 13. (Color online) Electronic DOS at the Fermi level for various metallic LiBeB phases and pressures. Here, as earlier, DOS is normalized per valence electron. "Global min" follows the low-enthalpy structures for various pressures. The electron gas DOS is calculated at all pressures for electron densities n corresponding to the *Ama2* structure, by using $\mathrm{DOS}(E_f) = 3/(2E_f)$ with the bandwidth $E_f \sim n^{2/3}$.

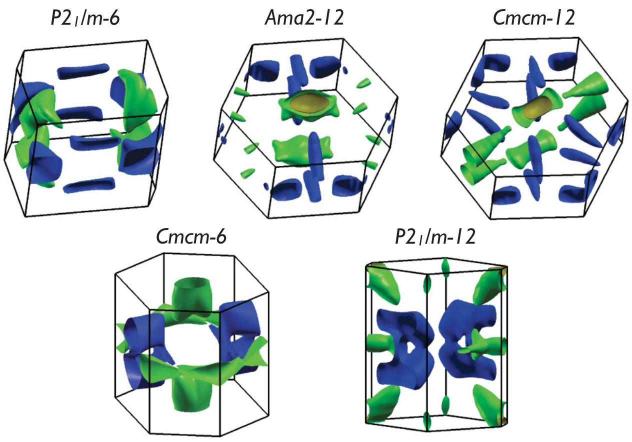

FIG. 14. (Color online) Fermi surfaces of various LiBeB phases at different pressures. From top left to lower right: (i) *P2₁/m-6* at P = 1 atm; (ii) *Ama2-12* at P = 40 GPa; (iii) *Cmcm-12* at P = 40 GPa; (iv) *Cmcm-6* at P = 160 GPa; (v) *P2₁/m-12* at P = 160 GPa. Brillouin zones are not drawn to scale. Blue (dark gray), green (light gray), and yellow (medium gray) sheets denote the first, second, and third band crossing the Fermi level, respectively.

The Debye temperature T_D is estimated using the relation

$$T_D = \hbar c k_D, \quad \text{with} \quad c = \sqrt{B_0/\rho} \quad \text{and} \quad \frac{4\pi}{3}k_D^3 = (2\pi)^3 n,$$

where c is the speed of sound, ρ is the mass density, and n is the atom density, which determines the Debye wave vector k_D. The bulk modulus B_0 is obtained from equation-of-state fits to the energy-volume relation $E(V)$ for each phase. The pressure dependence of these Debye temperatures is shown in Fig. 15, together with the T_D values for the elemental phases of Li, Be, and B, and their experimental values at atmospheric pressure.

All LiBeB phases show a rapid increase of T_D under pressure, driven by a reduced compressibility (i.e., increased bulk modulus) that outweighs the net inverse proportionality on the material density. The experimental values of T_D for elemental Li, Be, and B at atmospheric pressures are reproduced reasonably well, and up to P = 40 GPa, the ternary compounds are "sandwiched" between the "soft" Li and the "hard" Be and B. Note that all compact LiBeB phases show very similar dynamical properties in this respect, independent of the detailed atomic arrangement. In contrast, the layered *P2₁/m-6* structure shows a much more rapid increase of T_D with pressure, up to P = 25 GPa, when it undergoes a phase transition to the *Cmcm-6* structure.

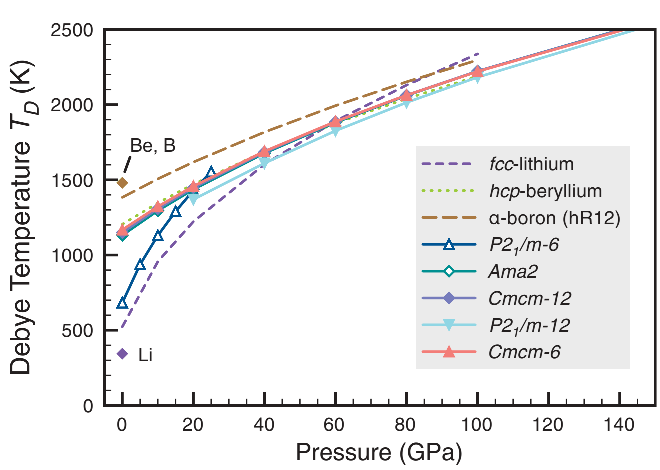

FIG. 15. (Color online) Debye temperatures for various metallic LiBeB phases (solid lines with symbols), elemental crystals (dashed lines), and experimental values (diamond symbols and labels). Note that on this scale, Be and B have indistinguishable experimental Debye temperatures.

Estimated transition temperatures for these structures (using McMillan's formula as cited earlier herein, and setting $\mu^* = 0.10$) are not very encouraging. We find rather small electron-phonon coupling parameters: $\lambda = 0.23$ for *P2₁/m-6*; $\lambda = 0.18$ for *Ama2*; and $\lambda = 0.23$ for *Cmcm-6*. Following the most stable metallic phases, we obtain $T_c = 10$ mK for the *P2₁/m-6* phase at P = 1 atm; $T_c = 0$ for the *Ama2* phase at P = 40 GPa; and $T_c = 10$ mK for the *Cmcm-6* phase at P = 160 GPa. Recall that T_c for pure Be is 26 mK.

XII. SUMMARY

We present here calculations on 1:1:1 LiBeB, to date an unknown phase. By tuning the external pressure, we predict a sequence of stable phases characterized by very different structural motifs, ranging from layered structures, via ternary variants of hexagonal Laves phases (with helices in them), to intricately "colored" body-centered cubic structures. We expect in LiBeB a metal-to-insulator transition at a pressure of P = 70 GPa, where the body-centered structures first become stable. The material will return at still higher pressures to being metallic. Neither the DOS at the Fermi level, nor the electron-phonon coupling in these structures is encouraging for high-T_c superconductivity. A major and persistent difficulty is the pseudogap character of the density of states near the Fermi energy.

The electron distribution in all phases follows electronegativity considerations—The lithiums effectively transfer electrons to the borons, and the states near the Fermi level are mostly on the beryllium atoms. In fact, some of the high-pressure phases have a DOS quite similar in nature to that of Be metal. In one of the high-pressure phases, we see a Dirac point near the Fermi energy, actually a two-dimensional surface of such points. Predicted to be stable thermodynamically at P = 1 atm and some higher pressures, LiBeB, while not likely to be a superconductor, has some remarkable and instructive structural and electronic features.

ACKNOWLEDGMENTS

Our work was supported by EFree, an Energy Frontier Research Center funded by the US Department of Energy (Award Number DESC0001057 at Cornell) and the National Science Foundation through grants CHE-0910623 and DMR-0907425. Computational resources provided by the Cornell NanoScale Facility (supported by the National Science Foundation through grant ECS-0335765), and by the TeraGrid network (provided by the National Center for Supercomputer Applications through grant TG-DMR060055N), are gratefully acknowledged.

APPENDIX: COMPUTATIONAL DETAILS

Prediction of crystal structures of systems of a given chemical composition is well recognized as an exceedingly difficult task.[59] This is even more complicated if one moves from the familiar conditions of P = 1 atm, amenable to chemical synthesis and intuition, to high applied pressures.[60] An efficient sampling of the rich crystalline configurational space must therefore be performed to detect potential ground-state structures. Here this is achieved by utilizing an evolutionary algorithm approach,[61–64] as implemented in the XtalOpt package.[65] Optimized structures and energies are obtained through density functional theory as programmed in a plane wave formalism in the VASP package,[66] using the Perdew-Burke-Ernzerhof parameterization of the electronic exchange-correlation energy,[67] and the Projector Augmented Wave (PAW) method to describe the electron-ion interaction.[68,69] Structure searches were performed at P = 1 atm, 40 GPa, 80 GPa, 160 GPa, and 320 GPa, using standard PAW data sets for the atoms (which include 2s and 2p valence electrons) and a plane wave energy cutoff of $E_c = 400$ eV. Low-energy candidate structures were then reoptimized across the whole pressure range using all-electron PAW data sets for lithium and beryllium, a "hard" data set for boron (cutoff radii 1.6, 1.8, and 1.1a_0, respectively), and an energy cutoff of $E_c = 800$ eV. Enthalpies of formation of ternary structures were calculated with respect to known atomic structures of lithium, beryllium, and boron as well as the computed and known binary phases made up of the these elements. Zero point energies (ZPE's) were not included in the determination of stable phases. Typical ZPE's, obtained in the quasi-harmonic approximation, range from 0.27 eV per formula unit in the $P2_1/m$-6 structure at P = 1 atm to 0.58 eV per formula unit in the $P3m1$ structure at P = 320 GPa.

Estimates of the transition temperatures to superconductivity were obtained using the Allen-Dynes modification of McMillan's formula[70,71] as implemented in the QUANTUM ESPRESSO code,[72] and utilizing ultrasoft pseudopotentials[73] for Li, Be, and B from www.quantum-espresso.org.

*ah736@cornell.edu

[1] E. Wigner and H. B. Huntington, J. Chem. Phys. **3**, 764 (1935).
[2] N. W. Ashcroft, Phys. Rev. Lett. **21**, 1748 (1968).
[3] M. I. Eremets and I. A. Troyan, Nat. Mater. **10**, 927 (2011).
[4] André Kietzmann, Bastian Holst, Ronald Redmer, Michael P. Desjarlais, and Thomas R. Mattsson, Phys. Rev. Lett. **98**, 190602 (2007).
[5] P. M. Kowalski, S. Mazevet, D. Saumon, and M. Challacombe, Phys. Rev. B **76**, 075112 (2007).
[6] S. A. Khairallah and B. Militzer, Phys. Rev. Lett. **101**, 106407 (2008).
[7] Lars Stixrude and Raymond Jeanloz, Proc. Natl. Acad. Sci. USA **105**, 11071 (2008).
[8] P. M. Celliers, P. Loubeyre, J. H. Eggert, S. Brygoo, R. S. McWilliams, D. G. Hicks, T. R. Boehly, R. Jeanloz, and G. W. Collins, Phys. Rev. Lett. **104**, 184503 (2010).
[9] Eva Zurek, Roald Hoffmann, N. W. Ashcroft, Artem R. Oganov, and Andriy O. Lyakhov, Proc. Natl. Acad. Sci. **106**, 17640 (2009).
[10] Kazutaka Abe and N. W. Ashcroft, Phys. Rev. B **84**, 104118 (2011).
[11] Yansun Yao and Roald Hoffmann, J. Am. Chem. Soc. **133**, 21002 (2011).
[12] A. Züttel, P. Wenger, S. Rentsch, P. Sudan, Ph. Mauron, and Ch. Emmenegger, J. Power Sources **118**, 1 (2003).
[13] S. Orimo, Y. Nakamori, G. Kitahara, K. Miwa, N. Ohba, S. Towata, and A. Züttel, J. Alloy. Compd. **404–406**, 427 (2005).
[14] Nobuko Ohba, Kazutoshi Miwa, Masakazu Aoki, Tatsuo Noritake, Shin-ichi Towata, Yuko Nakamori, Shin-ichi Orimo, and Andreas Züttel, Phys. Rev. B **74**, 075110 (2006).
[15] Yuko Nakamori, Kazutoshi Miwa, Akihito Ninomiya, Haiwen Li, Nobuko Ohba, Shin-ichi Towata, Andreas Züttel, and Shin-ichi Orimo, Phys. Rev. B **74**, 045126 (2006).
[16] A. N. Kolmogorov, R. Drautz, and D. G. Pettifor, Phys. Rev. B **76**, 184102 (2007).
[17] V. Ozolins, E. H. Majzoub, and C. Wolverton, J. Am. Chem. Soc. **131**, 230 (2009).
[18] Dasari L. V. K. Prasad, Musiri M. Balakrishnarajan, and Eluvathingal D. Jemmis, Phys. Rev. B **72**, 195102 (2005).
[19] Matteo Calandra, Aleksey N. Kolmogorov, and Stefano Curtarolo, Phys. Rev. B **75**, 144506 (2007).
[20] A. Lazicki, Russell J. Hemley, W. E. Pickett, and Choong-Shik Yoo, Phys. Rev. B **82**, 180102 (2010).
[21] Hsin Lin, L. Andrew Wray, Yuqi Xia, Suyang Xu, Shuang Jia, Robert J. Cava, Arun Bansil, and M. Zahid Hasan, Nat. Mater. **9**, 546 (2010).
[22] Tanja Graf, Claudia Felser, and Stuart S. P. Parkin, Prog. Solid State Chem. **39**, 1 (2011).
[23] Jun Nagamatsu, Norimasa Nakagawa, Takahiro Muranaka, Yuji Zenitani, and Jun Akimitsu, Nature **410**, 63 (2001).
[24] Timothy Hughbanks, J. Am. Chem. Soc. **107**, 6851 (1985).
[25] Nobuhiko Kato, Hidemi Nagao, Kiyoshi Nishikawa, Kazume Nishidate, and Kazunaka Endo, Int. J. Quant. Chem. **96**, 457 (2004).
[26] See Supplemental Material at http://link.aps.org/supplemental/10.1103/PhysRevB.86.014104 for crystal structures, geometrical, and bonding analyses of the phases of LiBeB.
[27] D. J. Fredeman, P. H. Tobash, M. A. Torrez, J. D. Thompson, E. D. Bauer, F. Ronning, W. W. Tipton, Sven P. Rudin, and R. G. Hennig, Phys. Rev. B **83**, 224102 (2011).
[28] J. Christian Schön and Martin Jansen, Angew. Chem., Int. Ed. **35**, 1286 (1996).
[29] Martin Jansen, Angew. Chem., Int. Ed. **41**, 3746 (2002).
[30] Martin Jansen, Ilya V. Pentin, and J. Christian Schön, Angew. Chem., Int. Ed. **51**, 132 (2012).
[31] Ji Feng, Richard G. Hennig, N. W. Ashcroft, and Roald Hoffmann, Nature **451**, 445 (2008).
[32] P. Villars, H. Okamoto, and K. Cenzual, *ASM Alloy Phase Diagrams Center* (ASM International, Materials Park, OH, 2006).
[33] H. Okamoto and L. E. Tanner, in *Binary Alloy Phase Diagrams*, 2nd ed., edited by T. B. Massalski, H. Okamoto, P. R. Subramanian, and L. Kacprzak (ASM International, Materials Park, OH, 1990), p. 460.

[34]H. B. Borgstedt and C. Guminski, J. Phase Equilib. **24**, 572 (2003).
[35]Michael Wörle and Reinhard Nesper, Angew. Chem., Int. Ed. **39**, 2349 (2000).
[36]Zhijian Liu, Xuanhui Qu, Baiyun Huang, and Zhiyou Li, J. Alloy. Compd. **311**, 256 (2000).
[37]A. F. Wells, J. Chem. Soc. **69**, 1662 (1947).
[38]Albert W. Schlueter, Robert A. Jacobson, and Robert E. Rundle, Inorg. Chem. **5**, 277 (1966).
[39]Boris Zemva, Karel Lutar, Adolf Jesih, William J. Casteel, Angus P. Wilkinson, David E. Cox, Robert B. Von Dreele, Horst Borrmann, and Neil Bartlett, J. Am. Chem. Soc. **113**, 4192 (1991).
[40]James B. Friauf, Phys. Rev. **29**, 34 (1927).
[41]Fritz Laves and H. Witte, Metallwirtsch. **14**, 645 (1935).
[42]F. Stein, M. Palm, and G. Sauthoff, Intermetallics **13**, 1056 (2005).
[43]F. C. Frank and J. S. Kasper, Acta Cryst. **11**, 184 (1958).
[44]E. Hellner and F. Laves, Z. Kristallogr. **105**, 134 (1943).
[45]K. J. Range, F. Rau, and U. Klement, Z. Naturforsch., B **45**, 1333 (1990).
[46]Reinhard Nesper and Gordon J. Miller, J. Alloy. Compd. **197**, 109 (1993).
[47]Ji Feng, N. W. Ashcroft, and Roald Hoffmann, Phys. Rev. Lett. **98**, 247002 (2007).
[48]Jeremy K. Burdett, Stephen Lee, and Timothy J. McLarnan, J. Am. Chem. Soc. **107**, 3083 (1985).
[49]Gordon J. Miller, Eur. J. Inorg. Chem. **1998**, 523 (1998).
[50]Jeremy K. Burdett, *Chemical Bonding in Solids* (Oxford University Press, New York, 1995).
[51]David C. Lonie and Eva Zurek, Comput. Phys. Commun. **183**, 690 (2012).
[52]Roy L. Johnston and Roald Hoffmann, Z. Anorg. Allg. Chem. **616**, 105 (1992).
[53]Lorin X. Benedict, Tadashi Ogitsu, Andrea Trave, Christine J. Wu, Philip A. Sterne, and Eric Schwegler, Phys. Rev. B **79**, 064106 (2009).
[54]W. J. Evans, M. J. Lipp, H. Cynn, C. S. Yoo, M. Somayazulu, D. Häusermann, G. Shen, and V. Prakapenka, Phys. Rev. B **72**, 094113 (2005).
[55]Xiangang Wan, Ari M. Turner, Ashvin Vishwanath, and Sergey Y. Savrasov, Phys. Rev. B **83**, 205101 (2011).
[56]A. K. Geim and K. S. Novoselov, Nat. Mater. **6**, 183 (2007).
[57]Joonbum Park, G. Lee, F. Wolff-Fabris, Y. Y. Koh, M. J. Eom, Y. K. Kim, M. A. Farhan, Y. J. Jo, C. Kim, J. H. Shim, and J. S. Kim, Phys. Rev. Lett. **107**, 126402 (2011).
[58]Kefeng Wang, D. Graf, Limin Wang, Hechang Lei, S. W. Tozer, and C. Petrovic, Phys. Rev. B **85**, 041101(R) (2012).
[59]John Maddox, Nature **335**, 201 (1988).
[60]Wojciech Grochala, Roald Hoffmann, Ji Feng, and Neil W. Ashcroft, Angew. Chem., Int. Ed. **46**, 3620 (2007).
[61]Bernd Hartke, J. Phys. Chem. **97**, 9973 (1993).
[62]Roy L. Johnston, Dalton Trans. 4193 (2003).
[63]Behnam Assadollahzadeh, Philip R. Bunker, and Peter Schwerdtfeger, Chem. Phys. Lett. **451**, 262 (2008).
[64]Artem R. Oganov, Andriy O. Lyakhov, and Mario Valle, Acc. Chem. Res. **44**, 227 (2011).
[65]David C. Lonie and Eva Zurek, Comput. Phys. Commun. **182**, 372 (2011).
[66]G. Kresse and J. Furthmüller, Phys. Rev. B **54**, 11169 (1996).
[67]John P. Perdew, Kieron Burke, and Matthias Ernzerhof, Phys. Rev. Lett. **77**, 3865 (1996).
[68]P. E. Blöchl, Phys. Rev. B **50**, 17953 (1994).
[69]G. Kresse and D. Joubert, Phys. Rev. B **59**, 1758 (1999).
[70]P. B. Allen and R. C. Dynes, J. Phys. C **8**, L158 (1975).
[71]W. L. McMillan, Phys. Rev. **167**, 331 (1968).
[72]Paolo Giannozzi, Stefano Baroni, Nicola Bonini, Matteo Calandra, Roberto Car, Carlo Cavazzoni, Davide Ceresoli, Guido L. Chiarotti, Matteo Cococcioni, Ismaila Dabo, Andrea Dal Corso, Stefano De Gironcoli, Stefano Fabris, Guido Fratesi, Ralph Gebauer, Uwe Gerstmann, Christos Gougoussis, Anton Kokalj, Michele Lazzeri, Layla Martin-samos, Nicola Marzari, Francesco Mauri, Riccardo Mazzarello, Stefano Paolini, Alfredo Pasquarello, Lorenzo Paulatto, Carlo Sbraccia, Alexander Smogunov, Paolo Umari, and Renata M. Wentzcovitch, J. Phys. Condens. Matter **21**, 395502 (2009).
[73]David Vanderbilt, Phys. Rev. B **41**, 7892 (1990).